TOWARDS A MOBILE MOTION ANALYSIS LABORATORY: IMPROVEMENTS IN WEARABLE MOTION CAPTURE AND FORCE MEASUREMENT

by

Lucas Samuel Lincoln

A thesis submitted to the faculty of
The University of Utah
in partial fulfillment of the requirements for the degree of

Master of Science

Department of Mechanical Engineering

The University of Utah

May 2012

The University of Utah Graduate School

STATEMENT OF THESIS APPROVAL

The thesis of **Lucas Samuel Lincoln**

has been approved by the following supervisory committee members:

Stacy Bamberg	, Chair	**12/07/2011** Date Approved
Donald Bloswick	, Member	**12/07/2011** Date Approved
Bruce MacWilliams	, Member	**12/07/2011** Date Approved
Jason Wheeler	, Member	**12/07/2011** Date Approved

and by **Timothy Ameel** , Chair of the Department of **Mechanical Engineering**

and by Charles A. Wight, Dean of The Graduate School.

ABSTRACT

Gait analysis is an important tool for diagnosing a wide variety of disorders, with its increasingly accepted benefits culminating in the widespread adoption of motion analysis laboratories. A modern analysis laboratory consists of a multicamera marker tracking system for 3D reconstruction of kinematics and multiple high-fidelity load transducers to determine ground reaction force and enable inverse-dynamics for biomechanics. There is a need for an alternative motion analysis system which does not require a fixed laboratory setting and is lower in cost; freeing the motion capture from the laboratory and reducing the technology costs would enable long-term, home-based, natural monitoring of subjects.

This thesis describes two contributions to the end goal of an inexpensive, mobile, insole-based motion analysis laboratory. First is the application of an inertial-measurement-unit calibration routine and zero-velocity-update algorithm to improve position and orientation tracking. Second is the development, from basic sensor to prototype, of an insole capable of measuring 3 degree-of-freedom ground reaction force. These contributions represent a proof-of-concept that quantitative gait analysis, complete with dynamics, is possible with an insole-based system.

To my grandfather Arthur Dalton, who showed me that you can,
and must, do everything with a smile.

TABLE OF CONTENTS

LIST OF TABLES

LIST OF FIGURES

CHAPTER 1

INTRODUCTION

This section presents the motivation for human motion analysis and proposed benefits of a mobile motion analysis laboratory (MAL) over traditional systems. The previous research is reviewed prior to stating contributions and current research.

1.1 Background

Human gait is the primary form of personal locomotion and a large contributing factor in an individual's quality of life and independence. Because of this, and the prevalence of a variety of gait disorders [1], there has been significant research into quantitative motion analysis, with particular activity since the 1970s. In the 1970s and 1980s, video camera systems were deployed which enabled 3-dimensional kinematics tracking and dynamic analysis when coupled with floor-mounted force plates or instrumented treadmills. This type of motion analysis laboratory enabled physicians to perform studies and diagnose pathologies for individual patients [2][3].

There is a commonality in the modern motion analysis lab, and though there are exceptions, a typical MAL today will contain:

1. A passive or active marker and camera system for tracking movements.

2. Load transducers for measuring ground reaction force (GRF) and center of pressure (CoP).
3. Electromyogram electrode systems for approximation of individual muscle activation levels.

With data from the first two items, it is possible to use inverse dynamics (via the Newton-Euler equations of motion) to compute the loads and torques at the subject's joints, an important piece of clinical gait analysis.

With full inverse dynamics, experienced clinicians alter their initial, premotion analysis treatment suggestions 52%-89% of the time, typically reduce the number of surgeries performed and risk therein, and in general produce more improved outcomes for patients [4].

The benefits of human gait analysis are now rarely argued against, and the previously described type of analysis and laboratory equipment is the gold standard for diagnosing human gait disorders; however, there are a few evident shortcomings manifesting from the technologies used. Simply: the equipment is, for most purposes, fixed to the laboratory setting and, in addition, contains significant costs.

Multicamera motion capture systems rely on direct-linear transformations to perform 3D reconstruction of the markers in space. This is a function of the geometry of the cameras and requires each marker to be viewed by at least 2 cameras at any given time. Typically, due to limitations in viewing from any particular vantage, a MAL will be outfitted with 6-12 cameras surrounding the subject. This defines a volume in the center in which kinematics capture can take place. Motion capture outside the laboratory would require setting up this system of cameras and recalibrating them using marker sets of

known geometries. This is not feasible for most clinical motion capture, and combined with the fixed location of the load cells, limits gait analysis to a laboratory or hospital setting.

The second issue with current MAL setups is the high cost. The costs associated with a current gait analysis lab were estimated above $300,000 for initial setup and $50,000-$300,000/year in the year 2004 [4]. The videocameras require high-bandwidth connections back to a high-performance computer for computation of 3D motion; and load cells are often on the order of $1,000-$10,000 [5].

The author proposes that addressing these two issues by developing new technologies will provide clinicians and physicians with greater tools to understand, diagnose, and prevent gait disorders. It is believed that instrumentation for mobile and low-cost motion analysis will result in long-term and ubiquitous study of subjects, improving the quantity and quality of data by capturing natural motions in common environments.

To enable freedom from a laboratory setting, the device or devices should be free of external-reference requirements, such as cameras or magnetic sensors. Additionally, for low-cost, the system should not require high-cost manufacturing techniques or sophisticated sensor systems. A wearable system using commonly available components is suggested.

1.2 Previous Work

The need for a lower cost, less restricted system for motion analysis was proposed ten years ago in the form of instrumentation for a shoe [6]. The instrumentation

consisted of a resistive bend sensor to measure plantar- and dorsiflexion of the foot, a 3 axis angular rate gyroscope, a 3 axis accelerometer, force-sensitive resistors (FSR) for stride timing, sonar sensors for step height, and an electric field sensor for the same purpose. This system, and those similar to it [7][8][9], provided primarily gait phase detection and timing statistics and did not enable full inverse-dynamics calculation. The reasons for this are the system's inability to measure force accurately (FSRs are inaccurate and nonlinear, and only measure force in one direction) and an inability to accurately determine motion in 3D for any period of time.

Advances in the quality of micro-electromechanical (MEMS) inertial measurement units (IMU) have caused significant and varied research into their application for motion tracking (see Chapter 2, Section 1.) This approach for motion tracking is currently in the commercial world; however, current companies suggest their products only provide 3D orientation, acceleration, and angular velocity [10,11]

Less active is the field of research in achieving true 3 degree-of-freedom measurement in a wearable system, though its importance to clinical gait analysis is equally significant. A review of the current state of insole GRF measurement can be found in Chapter 4, Section 1. In summary, the most accurate and mature current approaches use load cells replacing or augmenting the sole of a shoe, such as that of XSens Technologies ForceShoe. An instrumented shoe introduces uncertainty about alteration from a subject's natural gait and adoption in subjects due to the lack of transparency and deviation from their preferred sneaker. Perhaps most importantly, however, is the fact that the shoes measure the force and torques at the shoes sole, not at

the foot, as a gait lab does (subjects are typically tested barefoot on the forceplate) and an insole is proposed to do.

1.3 Contributions

Contributions contained in this thesis fall into two primary categories: the contributions to IMU motion tracking and the contributions to ground reaction force measurement in an insole.

In terms of IMU motion tracking, this thesis describes the application of a novel calibration system to low-cost IMUs. Physical experiments were performed in a motion analysis laboratory and the data were analyzed iteratively with different calibrations to determine the stability of the calibration system over time, with unique combinations of state-estimation (on/off) and calibration (user calibrations and factory) to determine the relative benefit of each aid to motion tracking. Additionally, absolute performance was evaluated over 5 trials with successful motion tracking.

Insole GRF contributions begin at the design and development of the tactile sensor. A novel sensor was developed using the design process of: design, construct, evaluate, redesign, and repeat. Numerous iterations of the tactile sensor where manufactured and evaluated, software was written for data capture, and analysis and an algorithm was developed to estimate force from the variety of signals produced by the hardware. Linear regression was used to train a variety of sensor models (linear, square, and cubic signal models, and those containing signal derivatives and combinations) and a linear model was found to be sufficient.

A physical sensor testing protocol was developed and the required tools (3 axis linear stage with distance encoders and 6DOF force measurement) was designed and constructed using primarily off-the-shelf components.

Adapting the validated tactile sensor to an insole was performed. A flex circuit was constructed and the silicone molding process for required optical geometries was defined and executed. A complete insole was produced and exponents performed in a motion analysis lab to evaluate performance. The concept that 3DOF GRF can be measured in a low-cost insole was proven successfully from design of principle sensor operation to construction of functional prototype.

1.4 Overview

The following chapters in this thesis have been submitted, or have been prepared for submission, for inclusion in conferences and journals.

In Chapter 2, a journal publication is presented describing the application of the IMU toolset to human gait. This paper is accepted for publication in the OMICS Journal of Bioengineering and Biomedical Sciences; Special Issue on Emerging Technology for Use in Rehabilitation.

In Chapter 3, a conference publication is presented which details the development of the tactile sensor for 3 degree-of-freedom pressure measurement. This paper is submitted to the 2012 IEEE EMBC/RAS International Conference on Biomedical Robotics and Biomechatronics.

In Chapter 4, a conference publication is presented which describes the 3DOF GRF sensing insole. This paper is submitted to the 2012 IEEE EMBC/RAS International Conference on Biomedical Robotics and Biomechatronics.

In Chapter 5, the main conclusions of the thesis are presented, along with recommendations for future work.

1.5 References

[1] F. A. Rubino, "Gait disorders." The Neurologist, vol. 8, no. 4, pp. 254-262, 2002

[2] D.H Sutherland, "The evolution of clinical gait analysis: Part II," Kinematics, Gait & Posture, vol. 16, no. 2, pp. 159-179, October 2002, ISSN 0966-6362

[3] J. Perry, Gait Analysis: Normal and Pathological Function. Thorofare, NJ: Slack; 1992357

[4] S. R. Simon, "Quantification of human motion: gait analysis—benefits and limitations to its application to clinical problems," Journal of Biomechanics, vol 37, no. 12, pp. 1869-1880, December 2004, ISSN 0021-9290

[5] AMTI Force and Motion Control, 2011, www.atmi.biz.

[6] S.J. Morris, "Shoe-integrated sensor system for wireless gait analysis and real-time feedback," Proc 2nd joint EMBS/BMES Conference, October 23-26, 2002.

[7] I.P. Pappas, "A reliable gait phase detection system," IEEE Trans Neural Syst Rehabil Eng, vol. 9, no. 2, pp. 113-125, June 2001

[8] JM Hausdorff, "Footswitch system for measurement of the temporal parameters of gait," Journal of Biomechanics, vol. 28, no. 3, pp. 347-351 March 1995

[9] S. Bamberg, A.Y. Benbasat, D.M Scarborough, D.E. Krebs, J.A. Paradiso, "Gait analysis using a shoe-integrated wireless sensor system," Information Technology in Biomedicine, IEEE Transactions on , vol. 12, no. 4, pp. 413-423, July 2008

[10] Xsens MTw, 2011, http://www.xsens.com/en/movement-science/mtw

[11] Shimmer Research, Applications, 2011, http://www.shimmer-research.com/applications-2/kinematics

CHAPTER 2

TOWARDS LOW-COST MEMS IMU GAIT ANALYSIS: IMPROVEMENTS USING CALIBRATION AND STATE ESTIMATION

Lucas Samuel Lincoln, Eric Allen Johnson, and Stacy J. Morris Bamberg

Department of Mechanical Engineering, University of Utah

The paper is accepted for publication in the 2011 OMICS Journal of Bioengineering and Biomedical Sciences: Special Issue on Emerging Technology for Use in Rehabilitation.

Bioengineering & Biomedical Science

Lincoln et al. J Bioengineer & Biomedical Sci 2011, S1
http://dx.doi.org/10.4172/2155-9538.S1-006

Research Article Open Access

Towards Low-Cost Mems Imu Gait Analysis: Improvements Using Calibration and State Estimation

Lucas Samuel Lincoln, Eric Allen Johnson and Stacy J. Morris Bamberg

BioInstrumentation Laboratory, University of Utah, USA

Abstract

Inexpensive, unobtrusive 3D motion tracking of human gait is of increasing interest for the medical and entertainment industries. Of particular interest are rehabilitative applications. For instance, being able to measure foot travel, e.g. stride length or foot clearance, would be very useful. Approaches using low-cost MEMS inertial measurement units have often been limited by requiring expensive calibration procedures and by the sensor's inherent noise and bias drift. The authors apply two techniques to improve IMU based gait tracking: a novel calibration routine and a zero-velocity bias update algorithm. The application of these aids reduces error by an average of 99.55% over six trails. Results show a 5.96% tracking accuracy in the progressive direction, which corresponds to errors on the centimeter scale.

Introduction and Motivation

Human motion tracking and analysis is an active subject of study covering a large range of applications from healthcare to entertainment. Traditionally, human motion tracking has relied on external camera or magnetic systems, obtrusive instrumentation, or high cost equipment; a review of techniques may be found in [1]. In a clinical sense, the former both have the ability to influence analysis thought patient physical or mental discomfort, and the latter can be inhibiting to large-scale or long-term monitoring.

MEMS inertial measurement units (IMU), consisting of accelerometers and angular rate gyroscopes, have been applied to segment tracking for applications from the medical field to the entertainment industry [2-13]. IMUs have the benefit of being relatively small and unobtrusive, unlike instrumented linkages, and they are also self contained (requiring no specific environment for operation), unlike stereographic camera, vision, and magnetic tracking systems. Their mass adoption in the consumer electronics world has resulted in powerful sensors for continually decreasing cost and size. However, common problems exist in IMU use for segment tracking, predominantly the bias drift of the sensors and the non-linearities inherent in low-cost manufacturing, both of which notably introduce imperfect gravity cancellation [14].

Recent advances in real-time bias adjustment by the authors [15] as well as the development of a novel, inexpensive calibration system for low-cost IMUs [16], have encouraged a revisiting of the applicability of IMU gait analysis in general application, in particular with regard to accuracy and system cost.

The low-cost calibration of MEMS inertial sensors provides complex sensor models that account for scale factor nonlinearity, anisotropic sensitivity, and gyro specific force sensitivity [16].

This affords greater accuracy of measurement, particularly in estimating the required gravity cancellation. When double-integrating the acceleration signals for position even, small errors and unaccounted angular manufacturing tolerances can greatly affect the accuracy of tracking. This problem has typically limited the usefulness of IMU motion tracking for any real world tasks.

Our previous state estimation work [15] demonstrated that for human-scale, intermittent motion a sensor-level algorithm based on easily measured parameters enables real-time bias adjustment. This system is non-specific to application provided there are regular periods of rest. This has been demonstrated successfully on a small unmanned ground vehicle [16].

This paper investigates whether human gait provides long enough periods of rest to apply the state estimation algorithm for bias adjustment. This, combined with the calibration system developed, affords low-cost IMU based bioinstrumentation for human-motion tracking.

Materials and Methods

Inertial measurement unit

The IMU used is shown in Figure 1. Details of the sensor can be found in [16]. In short, the external dimensions are within 50 × 37 × 75 mm and it contains four independent accelerometer triads and two independent gyrotriads. The sensors are sampled at 1000Hz with a 16-bit A/D. The redundancy of the sensors allows for a weighted combination based on the static variance of each individual axis. At any time, saturated sensors are weighted out of the resulting signal.

Calibration

The calibration system previously developed, fully described in [16], and provides an average improvement of 5.7% and 24% over linear models for the accelerometers and gyros, respectively. This improves the state estimation described above, and combined they greatly reduce the compounding error resulting from multiple integrations over time. The calibration hardware is low cost and consists of a series of blocks manufactured to specific linear and angular dimensions (Figure 2). By exciting combinations of gyro- and accelerometer- axes through a predefined series of pure translational and rotational motions, a novel mathematical model is populated. This model includes non-

***Corresponding author:** Stacy J. Morris Bamberg, BioInstrumentation Laboratory, University of Utah, Salt Lake City, UT84101, E-mail: sjm.bamberg@utah.edu

Received November 06, 2011; **Accepted** November 21, 2011; **Published** November 22, 2011

Citation: Lincoln LS, Johnson EA, Bamberg SJM (2011) Toward Slow - Cost Mems Imu Gait Analysis: Improvements Using Calibration and State Estimation. J Bioengineer & Biomedical Sci S1:006. doi:10.4172/2155-9538.S1-006

Citation: Lincoln LS, Johnson EA, Bamberg SJM (2011) Toward Slow - Cost Mems Imu Gait Analysis: Improvements Using Calibration and State Estimation. J Bioengineer & Biomedical Sci S1:006. doi:10.4172/2155-9538.S1-006

linearities, anisotropic effects and gyro-acceleration sensitivity. The hardware is low-cost and the calibration straightforward; however 180 actions are required to define the model. This results in a calibration time of approximately 4-6 hours. For home or clinical healthcare, a 6 hour calibration at each use would severely limit the applicability and adoption of an IMU based motion tracking device. This paper investigates the temporal stability of IMU calibration, that is: will the device require recalibration at each use; and if not re-calibrated at each use, how much benefit is lost? It is proposed that if the calibration is relatively static then periodic human segment motion can be accurately captured using wearable IMUs that are calibrated prior to the first use.

State Estimator

The state estimator works as described in [16]. It is a method of zero-velocity update intended to be application inspecific and was originally developed for mobile robotics tracking in GPS deficient environments. Zero velocity updates use a still period to re-bias accelerometer and gyros to minimize cumulating integration errors; they are typically based on step detection (using simple feature detection in accelerometer and gyro- scope signals [17,18] or insole pressure measurement) and assume a no-slip condition with the ground. If a slip occurs, this error is accumulated for the remainder of the trial. The method described herein uses the measured noise parameters of the IMU to determine periods of still, therefore increasing the robustness of the system in irregular terrain and eliminating the no-slip requirement. The bias-adjusting estimator has two tunable parameters for both accelerometers and gyroscopes: the length of time a signal must drop into the noise band of the sensor before being considered a still period (rather than noise or other abnormalities) and what magnitude to consider the noise band. These parameters are optimized on a given trial and applied to the algorithm prior to execution.

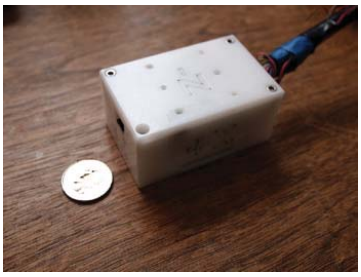

Figure 1: Photo of IMU, with US quarter for scale.

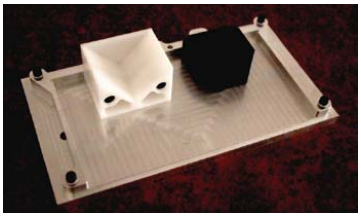

Figure 2: Photo of calibration hardware.

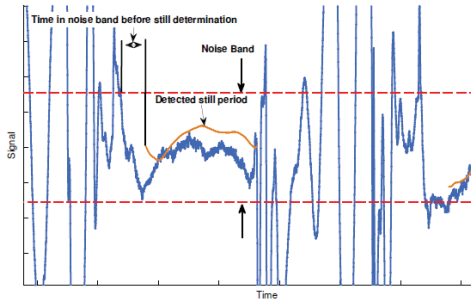

Figure 3: Still period detection on a representative trial showing tunable parameters of algorithm: Noise band and still period allowed prior to bias reset.

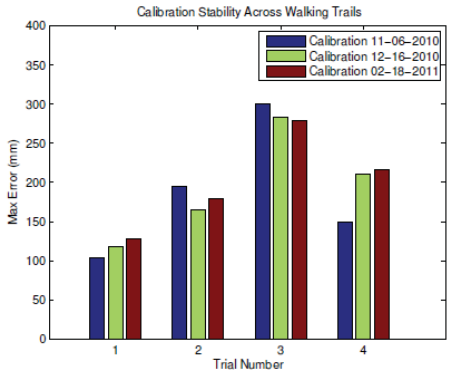

Figure 4: Graph showing relative stability of calibrations.

Experimental Procedure

Experiments were conducted in a motion analysis laboratory (MAL) which contains an 8-camera stereographic motion capture system (Vicon, Oxford, UK) for 3d motion tracking. The system has sub-millimeter accuracy and was utilized at a 1 kHz capture rate. The IMU was attached to the rigid cap of a steel-toed boot. Mounted securely to the IMU was an L shaped block with vision-system markers identifying the IMU coordinate system. The IMU is attached via a shielded cable to the DAQ system and powered by a constant DC power supply. Two types of trials were performed: Normal, unaffected gait on level ground (four trials) and natural stair climbing and descent of three steps (two trials). Both types of trails were used to examine calibration stability and the contributions of each aid (calibration and bias-update routine).

Analysis Methods and Techniques

A goal of this work was to determine the usefulness of the two tools (calibration and bias-update) and as such each gait trail was analyzed to determine the maximum error between IMU measurement and ground truth in a six configurations:

- Bias-update Off, Factory Calibration

Citation: Lincoln LS, Johnson EA, Bamberg SJM (2011) Toward Slow - Cost Mems Imu Gait Analysis: Improvements Using Calibration and State Estimation. J Bioengineer & Biomedical Sci S1:006. doi:10.4172/2155-9538.S1-006

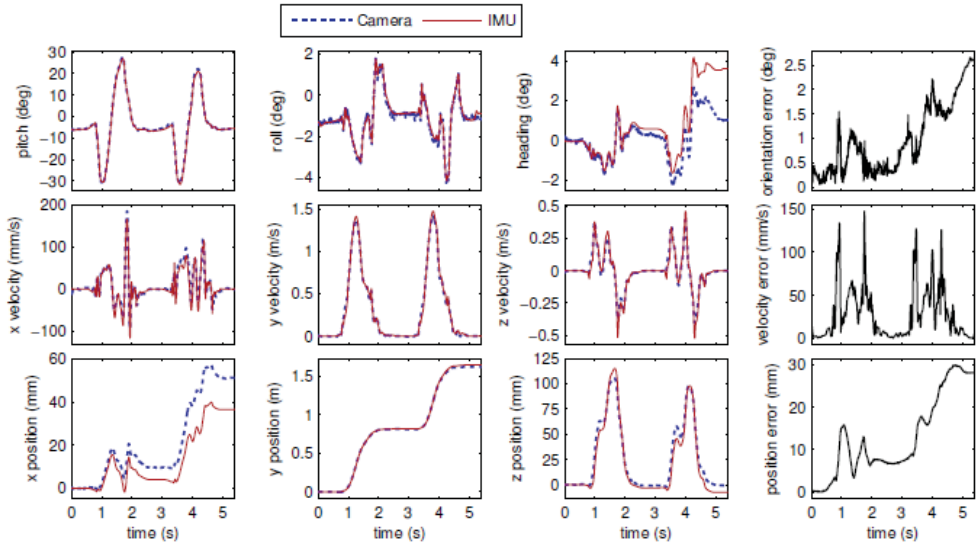

Figure 5: Plot showing IMU and camera tracking of the most accurate walking trial. Errors are in rightmost plots.

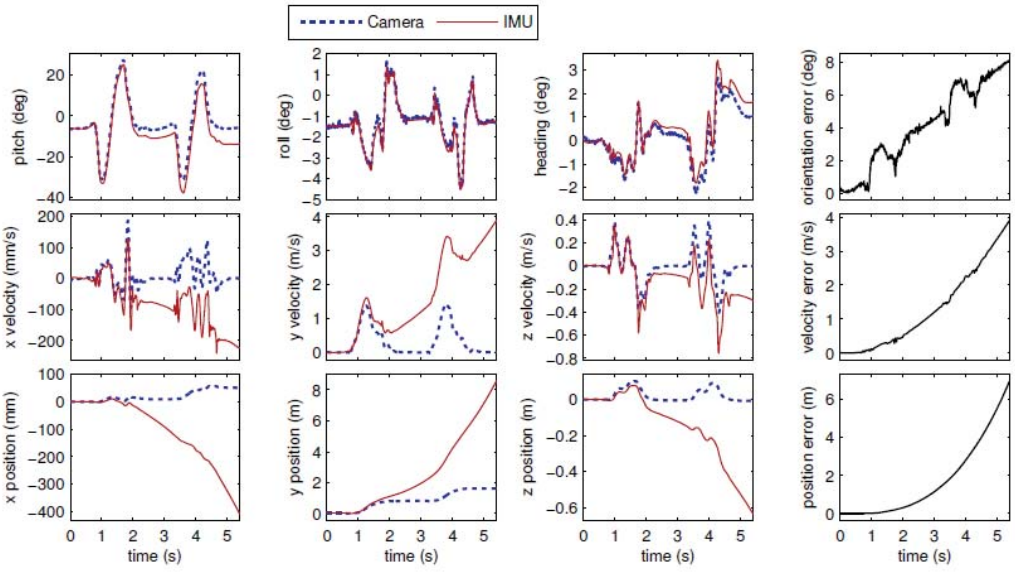

Figure 6: Plot showing same trial as Figure 5 with both calibration and state estimation aids removed. Note the rapidly compounding errors.

Citation: Lincoln LS, Johnson EA, Bamberg SJM (2011) Toward Slow - Cost Mems Imu Gait Analysis: Improvements Using Calibration and State Estimation. J Bioengineer & Biomedical Sci S1:006. doi:10.4172/2155-9538.S1-006

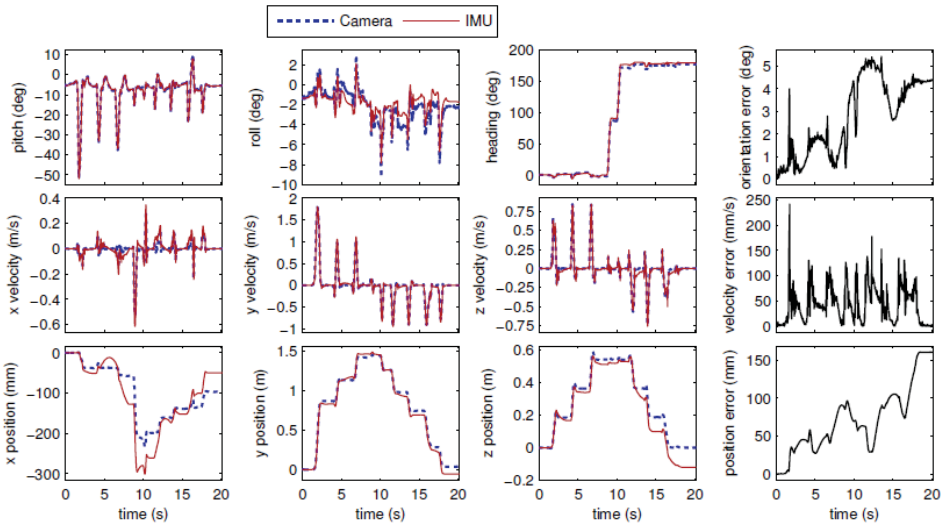

Figure 7: Plot showing IMU and camera tracking of a stairs trial. Errors are in right-most plots.

- Bias-update On, Factory Calibration
- Bias-update Off, User Calibration 1
- Bias-update On, User Calibration 1
- Bias-update On, User Calibration 2
- Bias-update On, User Calibration 3

This set of routines provides information as to the contribution of each tool; as well as providing an indication of the stability of calibrations by applying calibrations 1, 2 and 3 to the trails under otherwise identical conditions. Note calibrations 1 and 2 are from a common operator and 3 a different operator.

Results

To investigate the stability of calibration, Figure 4 demonstrates the relative difference in error by using three calibrations from different dates on the four walking gait trials. Likewise, to determine the relative effect of bias- adjustment and calibration, Table 1 displays the percent error reduction by applying our calibration routine, applying the bias-update algorithm; and applying both.

To determine the success of a low-cost IMU for gait tracking, all trials were analyzed with state estimation on and our calibration active. Figure 5 shows the angle, velocity, and position IMU tracking as well as truth from the camera system of a walking trial. Errors are shown in the rightmost plots. Figure 6 is the same trial as in 5 with both aids disabled, i.e. no bias updates and using the factory calibration. Figure 7 is a representative stairs trial. Table 2 contains the errors as a percentage of total distanced travelled, directionally for X, Y, Z and rotations. Y is the direction of primary progress in all trials, Z height, and X the lateral axis.

Discussion and Conclusions

The results are greatly improved by the process of calibrating and applying zero-velocity updates, as evidenced by comparing the representative stair (Figure 7) and gait (Figure 5) tracking results using the aids to the same walking trial without (Figure 6). The results Table 1 quantifies the improvement made by each aid. Note that state estimation alone makes the largest contribution to the error reduction; but also that the calibration improvements are non-trivial. The additional improvement of the calibration above state estimation alone is 104.75mm ± 163.82mm.

The low-cost, self calibration routine appears to be static across the walking trials as seen in Figure 4. The data does not show a trend for more recent calibrations to be more accurate, therefore a single, careful calibration to a new IMU is suspected to be sufficient for some months. Studies will continue with continuing calibration to further determine the stability of the parameters. Absolute errors as a percent of the distance travelled are shown in Table 2. Note that the mean error in the direction of progress is approximately 6%, with a particularly poor result in stair trial 2. The reason for this trial's poor performance has not been identified. The relatively larger error percentages in X and Z are in part due to the minimal amount of displacement in those directions. Their absolute errors are lower than those of the progressive direction.

Angular tracking is consistently strong across trials.

The work shown within demonstrates the vast error reduction in in-expensive IMU-based motion tracking made by using a low-cost, clinically feasible calibration routine as well as a bias-updating zero-velocity update algorithm. 3D tracking has been previously demonstrated to achieve errors under 1% [4,19], however this work uses more costly, and high-performance gyroscopes. A goal of this

Citation: Lincoln LS, Johnson EA, Bamberg SJM (2011) Toward Slow - Cost Mems Imu Gait Analysis: Improvements Using Calibration and State Estimation. J Bioengineer & Biomedical Sci S1:006. doi:10.4172/2155-9538.S1-006

Trial	Calibration	State Estimation	Both
Stairs 1	32.92%	99.92%	99.95%
Stairs 2	56.84%	99.57%	99.60%
Walking 1	33.03%	99.01%	99.65%
Walking 2	82.35%	97.51%	99.23%
Walking 3	88.15%	99.45%	99.46%
Walking 4	75.83%	99.29%	99.43%

Table 1: Aid effects, as percent reduction of the error with no state estimation and with factory calibration.

	Position Errors (%)			Angular Errors (%)		
Trial	X	Y	Z	X	Y	Z
Stairs 1	15.77	3.05	7.40	1.63	1.03	0.68
Stairs 2	17.45	20.30	9.25	1.55	1.06	1.01
Walking 1	12.44	1.47	2.88	5.34	0.63	0.72
Walking 2	21.81	3.68	21.59	1.22	1.31	0.83
Walking 3	27.20	3.74	10.90	3.72	1.18	0.48
Walking 4	14.30	3.52	13.05	1.38	1.27	0.74
Mean	18.16	5.96	10.85	2.47	1.08	0.74

Table 2: Errors as a percent of distance travelled.

work is to achieve reasonable results without requiring expensive equipment.

Future work will include larger scale studies of gait using IMUs and validation of the technique. Incorporation of the IMU into a removable insole and application of on-board digitization and wireless transfer will both improve the accuracy of the results and the ease of use. This will enable application for rehabilitation, for instance: to track distance traveled or to provide real-time feedback to improve gait and stride length. Rehabilitation to improve range of motion is also of interest.

References

1. Zhou H, Hu H (2008) Human motion tracking for rehabilitation-a survey, Biomed signal Process Control 3: 1-8.
2. E. Foxlin (1996) Inertial head-tracker sensor fusion by a complementary separate-bias Kalman filter. IEEE Virtual Reality Annual Int. Symposium (VRAIS'96) 185–194,267
3. E. Foxlin, M. Harrington, Y. Altshuler (1998) Miniature 6-DOF inertial system for tracking HMDs, in Proc. SPIE Conf. on Helmet- and Head- Mounted Displays III, vol. 3362, (Orlando, FL, USA) 214–228, Apr. 13–14.
4. Foxlin E (2005) Pedestrian tracking with shoe-mounted inertial sensors. IEEE Comput Graph Appl 25: 38-46.
5. Bamberg SJ, Benbasat AY, Scarborough DM, Krebs DE,Paradiso JA (2008) Gait analysis using a shoe-integrated wireless sensor system. IEEE Trans Inf Technol Biomed 12: 413-423.
6. Yang J, Choi ES, Chang W, Bang WC, Cho SJ, et al. (2004) A novel hand gesture input device based on inertial sensing technique. IEEE Industrial Electronics Society 30th Annual Conf. (IECON'04) 3: 2786–2791.
7. Zhu R, Zhou Z (2004) A real-time articulated human motion tracking using tri-axis inertial/magnetic sensors package, IEEE Trans Neural Syst Rehabil Eng12: 295-302.
8. Goodvin C, Park EJ, Huang K, Sakaki K (2006) Development of a real-time three-dimensional spinal motion measurement system for clinical practice, Med Biol Eng Comput 44: 1061-1075.
9. Luinge HJ, Veltink PH (2005) Measuring orientation of human body segments using miniature gyroscopes and accelerometers, Med Biol Eng Comput 43: 273-282.
10. Lee JK, Park EJ (2009) Minimum-order kalmanfilterwith vector se- lector for accurate estimation of human body orientation. IEEE Trans- actions on Robotics 25: 1196-1201.
11. Lee JK, Park EJ (2009) A fast quaternion-based orientation optimizer via virtual rotation for human motion tracking, IEEE Trans Biomed Eng 56: 1574-1582.
12. Miller N, Jenkins OC, Kallmann M, Mataric MJ (2004) Motion capture from inertial sensing for untethered humanoid teleoperation.. 4th IEEE-RAS Int. Conf. on Humanoid Robots 2: 547-565.
13. Wang JS, Hsu YL, Liu JN (2010) An inertial-measurement-unit- based pen with a trajectory reconstruction algorithm and its applica- tions, IEEE Transactions on Industrial Electronics 57: 3508-3521.
14. Woodman OJ (2007) An introduction to inertial navigation, Tech. Rep. 696, University of Cambridge, Computer Laboratory, 15 JJ Thomson Avenue, Cambridge CB3 0FD.
15. Johnson EA, Bamberg SJM, Minor MA (2008) A state estimator for rejecting noise and tracking bias in inertial sensors. IEEE Int. Conf. on Robotics and Automation (ICRA'08) 3256-3263.
16. Johnson EA (2011) Investigating inertial measurement for human-scale motion tracking. PhD thesis, University of Utah. Department of Mechanical Engineering.
17. Jimnez CPAR, Seco F, Guevara J (2009) A comparison of pedestrian dead-reckoning algorithms using a low-cost memsimu, in 6th IEEE International Symposium on Intelligent Signal Processing 37-42.
18. Ojeda L, Borenstein J (2007) Non-GPS navigation for security personnel and emergency responders. Journal of Navigation.
19. Foxlin E, Wan S (2010) Improved pedestrian navigation based on drift-reduced MEMS IMU chip, in ION International Technical Meeting. InterSense Incorporated.

This article was originally published in a special issue, **Emerging Technology for Use in Rehabilitation** handled by Editor(s). Dr. Philip Rowe, University of Strathclyde, UK

CHAPTER 3

AN OPTICAL 3D FORCE SENSOR FOR BIOMEDICAL DEVICES

Lucas Samuel Lincoln[1,2], Morgan Quigley[3], Brandon Rohrer[2] Curt Salisbury[2], and Jason Wheeler[2]

1. Department of Mechanical Engineering, University of Utah
2. Intelligent Systems and Controls, Sandia National Laboratories
3. AI Lab, Stanford University

This paper is submitted to the 2012 IEEE RAS/EMBS International Conference on Biomedical Robotics and Biomechatronics.

An optical 3D force sensor for biomedical devices

Lucas Samuel Lincoln, Morgan Quigley, Brandon Rohrer, Curt Salisbury, and Jason Wheeler

***Abstract*— In this paper we describe the development of an optical sensor that is low profile, inexpensive, physically robust, and suitable for contact with soft tissue. It is constructed using commercially available integrated circuits, a printed circuit board, and layers of silicone elastomer. The sensor exhibits modest drift and hysteresis, as well as some temperature sensitivity, for which we compensate. We demonstrate how the raw sensor signals can be used to infer both normal and shear forces. The sensor proves to be particularly sensitive to shear forces, reporting them accurately and with minimal coupling between them.**

I. INTRODUCTION

Low profile tactile sensors have been proposed for many applications including robot hands and skins [1], [2], [3] and biomechanical sensing at human/machine interfaces (e.g. in prosthetic sockets [4]). Many different types of tactile sensors have been proposed, including force sensitive resistors, which are available commercially, capacitive [4], optical [3], [2] and MEMS sensors. A recent review of tactile sensing can be found in Cutkosky, et al. [5].

The vast majority of the sensors in the research and patent literature sense normal loads (loads perpendicular to the sensing surface) but not shear loads (loads parallel to the sensing surface). For many applications, it would be beneficial to sense both. For instance in robotic hands, shear information could be used to improve object manipulation and tactile exploration. This information has also been shown to be important in monitoring prosthetic socket interface loads [6]. Multi-axis sensing has been primarily accomplished using traditional strain gauge-based load cells, which are typically large and expensive.

Several three-axis tactile sensors have been proposed. Capacitive sensors have been designed to infer shear information of overlapping conductors through a dielectric [4]. MEMS systems have been constructed with small cantilevers with piezo-resistive traces embedded in an elastomer [7], [8], [9]. These sensors have good sensing performance but have relatively small load capacity and are frail. Optical shear sensors have also been proposed. Missinnee et al. use a Vertical-Cavity Surface Emitting Laser which is mechanically separated from a photodiode by a silicone layer so that the two are displaced relative to one another by shear loads [10]. This sensor cannot sense normal pressure or easily differentiate between the two shear axes.

LS Lincoln is a student in the Bioinstrumentation Lab at the University of Utah, Salt Lake City, UT lucas.lincoln@utah.edu

M Quigley is a Ph.D. student in the AI Lab at Stanford University, Stanford, CA mquigley@cs.stanford.edu

B Rohrer, C Salibury, and J Wheeler are with Sandia National Laboratories, Intelligent Systems & Controls, Albuquerque, NM {rohrer, cmsalis, jwwheel}@sandia.gov

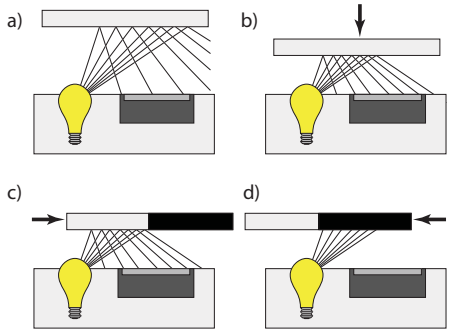

Fig. 1. The optical sensor's operating principle. a)-b) Normal loads move the reflective surface closer to the emitter, increasing the intensity of the light at the detector. c)-d) Shear loads move the absorptive portion of the polymer relative to the emitter, changing the intensity of the light at the detector.

In the present work, we present a three-axis optical sensor design which makes both normal and shear measurements. The sensor consists of small, inexpensive, surface-mount integrated circuits with multiple layers of silicone elastomer and is well suited for applications where a compliant material covers a rigid body (e.g. robot skins or prosthetic sockets).

II. SENSOR DESIGN

A. Principle of Operation

The sensor uses reflected light intensity to detect the proximity of a reflective material. As a normal load is applied to the reflective material, the interstitial transparent material compresses and the reflective material moves closer to the light source (emitter) and light sensor (detector). This causes the detector to detect increased reflected light from the emitter. (See Fig. 1a and 1b) Shear loads are sensed by adding absorptive regions to the reflective layer. An applied shear load changes the ratio of absorptive to reflective material between the emitter and the detector. The changes the amount of light reflected back to the detector. (See Fig. 1c and 1d)

Because each sensor configuration only provides information about a single degree of freedom, a *taxel* (from "tactile pixel") that provides three axes of information requires at least three sensors. Deducing the direction and magnitude of applied loads is most straightforward if the directional sensitivities of the three axes are independent.

B. Hardware and Implementation

The light emission and sensing were achieved using a photomicrosensor (EE-SY199, Omron Corporation, Kyoto,

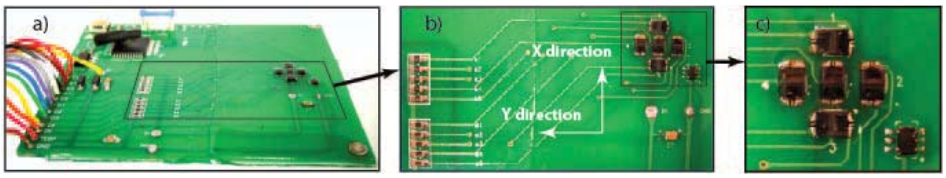

Fig. 2. Photograph of a five-sensor taxel (tactile sensing pixel). a) The entire printed circuit board, containing the sensors and the signal conditioning and preprocessing electronics. b) The sensors and their resistors. c) The photomicrosensor array, after coating with epoxy, but before coating with silicone. The center sensor is number 5. The chip to the lower right is a temperature sensor.

Japan) which contains both an infrared LED and phototransistor in the same package. This component was selected for its small size (approximately 3.2mm x 1.7mm x 1.1mm), wide-angle detection field, and the fact that its peak sensitivity occurs at approximately 1mm. We constructed a three-axis sensor consisting of five of these sensors: one which detected normal loads, two which detected shear in one direction, and two which detected shear in an orthogonal direction. (See Fig. 2) Initial characterization focused on the output from three of these sensors (2, 3, and 5), the simplest functional embodiment of the system. These sensors were cast in clear epoxy (ES1902 Hysol, Locktite, Henkel, Düsseldorf, Germany) up to the height of their top surface. A 1mm thick layer of transparent silicon (Dragon Skin Fast, Smooth-On, Inc., Easton, Pennsylvania) was used for the transparent resilient material. A thickness of 1mm of the same material was used for the opaque material, with a white die (White Silc Pig, Smooth-On, Inc., Easton, Pennsylvania) added to create the reflective surfaces and a black die (Black Silc Pig, Smooth-On, Inc., Easton, Pennsylvania) added to create the absorptive surfaces. A 6mm square was chosen for the geometry of the absorptive-reflective boundary. The reflective square was centered over the sensor for detecting normal loads. Two orthogonal boundaries of the square were placed directly over the two shear sensors (see Fig. 3). The opaque silicone was cast on top of the transparent silicone. Because the materials were similar silicone formulations, the interface bond was excellent. The silicone assembly was then bonded to the clear epoxy with a clear instant adhesive (Loctite 403, Henkel, Düsseldorf, Germany). Based on each sensor's field of view, it is estimated that taxels can be as close as 9 mm from center to center.

The datasheet for the sensor suggests a 4mA drive current for the LED. Given a supply voltage of 5V and a voltage drop across the LED of 1.2V, we used a 1kΩ current-limiting resistor in series with the LED to set the LED drive current to 3.8mA. We found through experiment that a load resistance of 100kΩ for the phototransistor with a 5V supply voltage gave us maximum sensitivity without saturating.

The sensors within a given taxel were close enough to one another that each phototransistor detected the cumulative reflected light from all of the LEDs. This secondary illumination saturated the phototransistors. To address this, we only drove one emitter at a time. The response time of the phototransistor was dependent upon the phototransistor

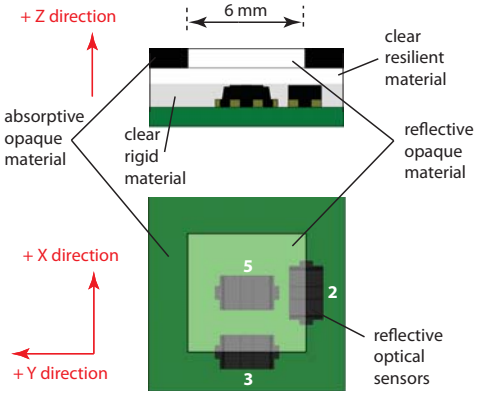

Fig. 3. Physical configuration of a single three-sensor taxel (sensors 1 and 4 from Figure 2 omitted). Changes in the reflected light intensity at the sensors allow measurement of normal and shear loads in three axes.

load resistance. Our 100kΩ resistor caused an exponential transient response with a 100μs time constant. In order to capture an accurate measurement from the phototransistor, we needed to wait until the phototransistor signal settled. Consequently, we set the LED pulses to be 1ms long. The phototransistor signal was sampled at 400μs, 500μs, 600μs and 700μs, and these four samples were averaged to generate a single phototransistor measurement (see Fig. 4). A single taxel measurement required measuring all three of the sensors and took a total of 3ms.

III. SENSOR CHARACTERIZATION

A. Method and Apparatus

A sensor designer and integrator is concerned about a variety of sensor characteristics when selecting a sensor for a particular application. We characterized several of these: the load sensitivity, hysteresis, drift, temperature sensitivity, and dynamic response of the prototype tactile sensor. All data were captured at 10kHz through a 16-bit National Instruments DAQ board (NI-PCI6229, National Instruments, Austin, TX). The data included the three photodetector analog signals and the three binary emitter states.

1) Load Sensitivity: We characterized the sensitivity of each of the three sensors in the taxel to normal and shear loads. To apply and measure shear and normal loads, we built and designed a test fixture (see Fig. 5) which consisted

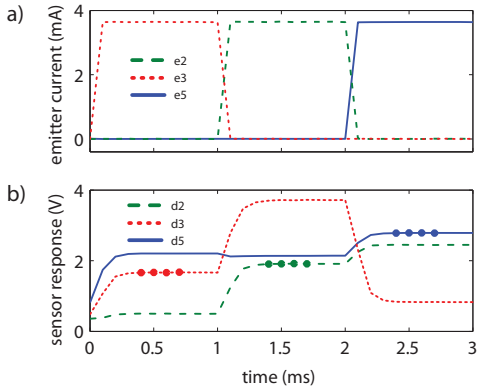

Fig. 4. Emitter-detector intensities. a) The LEDs were driven sequentially (emitter 3, emitter 2, then emitter 5). b) The photodetectors sensed the reflected intensity due to each. Note that in some instances another detector responded more strongly to an emitter than its own. (See for instance detector 3's response to emitter 2, the center plateau in the red trace.) Dots indicate the samples used to calculate a sensor value.

Fig. 5. The testing apparatus, including a three-axis linear stage, six-axis force transducer, and printed circuit board containing the three-axis tactile sensor.

of a three-axis linear stage (LT3, Thorlabs, Newark, NJ) attached to an optical breadboard and retrofitted with three optical encoders (S4-360-125-B-D, US Digital, Vancouver, WA) to record linear translation of the three stages ($<1\mu$m resolution). The optical encoder signals were sampled at 10kHz using a USB data-acquisition device (PhidgetEncoder, Phidgets, Calgary, Alberta, Canada). A six-axis load cell (Gamma US-30-100, ATI Industrial Automation, Apex, NC) was also rigidly attached to the breadboard, and the force and torque data were recorded through the same 16-bit NI DAQ board. The three-axis tactile sensor was mounted on top of the load cell. An effector plate attached to the stage applied loads to the top of the optical sensor through manual control of the linear stages.

Using this apparatus, we cycled stage displacements of approximately 1mm in a single direction (e.g. along the normal axis or one of the shear axes) at a time. Cycles were generated for all three directions and the sensor response was compared to the measured forces.

2) Cyclic Drift: To characterize the drift of the taxel output over time when driven by a cyclic load, we placed it in a single-axis load frame (MTS Systems Corp., Cary, NC) and loaded it in the normal direction. The load was cycled from 32 to 180kPa in a 0.5Hz triangle wave for approximately 2 hours. The MTS machine load cell data was recorded on the NI DAQ card.

3) Static Drift and Temperature Sensitivity: To characterize the static drift of the taxel, a 67N load with a contact area of 645mm^2 was placed on it, resulting in a sustained normal load. The sensor data were recorded for a period of 16 hours. Ambient thermal data were also recorded on the NI DAQ card.

4) Dynamic Response: To characterize the dynamic response of the taxel, it was positioned in a vise such that closing the jaws applied a normal load. The vice was then quickly closed on the taxel, resulting in a step-like response. Only sensor 5 was measured, with only its emitter on, for the duration of the experiment. In this fashion, we ensured that the sample rate was not limited by the serial sampling scheme for the three sensors.

5) Sensor modeling: With basic sensor characterization complete, data from all five sensors on the board were gathered for testing and validation. A five sensor arrangement resulted in a similarly sized taxel but provided redundant sensors for sensing shear, possibly increasing accuracy. Although the emitters were active only in pulses, the detectors were on continuously. The light from a single emitter could reach multiple detectors, providing additional information. With five sensors, each emitter pulse provided five values, and an entire pulse train (5ms at 1ms/pulse with five sensors) provided 25 signals. All 25 emitter-detector signals were captured while the sensor was subjected to complex three-dimensional loads. The system was trained using a linear-least-squares regression to determine coefficients (α) of the linear model:

$$\begin{aligned} p_x &= \alpha_{x1}D_1E_1 + \alpha_{x2}D_1E_2 + \alpha_{x3}D_1E_3 + ... \\ &\quad \alpha_{x23}D_5E_3 + \alpha_{x24}D_5E_4 + \alpha_{x25}D_5E_5 + \alpha_{x26} \\ p_y &= \alpha_{y1}D_1E_1 + \alpha_{y2}D_1E_2 + \alpha_{y3}D_1E_3 + ... \\ &\quad \alpha_{y23}D_5E_3 + \alpha_{y24}D_5E_4 + \alpha_{y25}D_5E_5 + \alpha_{y26} \\ p_z &= \alpha_{z1}D_1E_1 + \alpha_{z2}D_1E_2 + \alpha_{z3}D_1E_3 + ... \\ &\quad \alpha_{z23}D_5E_3 + \alpha_{z24}D_5E_4 + \alpha_{z25}D_5E_5 + \alpha_{z26} \end{aligned} \quad (1)$$

In the model notation, D_iE_j is the signal from detector i while illuminated by emitter j. Other models were tested as well: non-linear polynomial models up to the 3rd order and models incorporating the slope of the incoming signals. Performance was most consistent across trials with the linear least squares regression of Equation 1. For comparison, two reduced-order models were assessed as well. In a 5 signal model (Equation 2), detectors only reported on measurements made while their own emitter was active. These signals typically appeared to be the largest in magnitude and the most sensitive to changes in load.

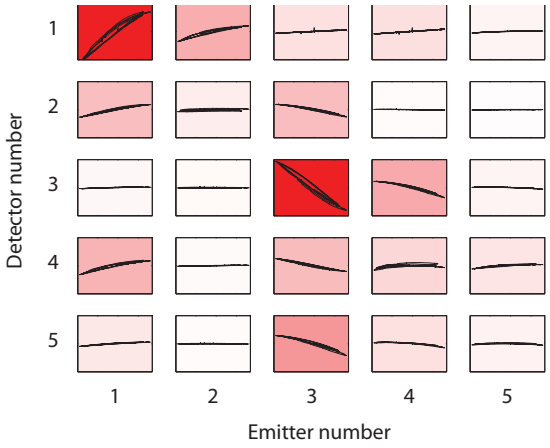

Fig. 6. Signal response to changing x load. Rows are detectors; Columns are emitters. x axis is pressure; y axis is signal voltage. Background color intensity represents sensitivity, also visible in the overall slope of each line.

$$\begin{aligned} p_x &= \alpha_{x1}D_1E_1 + \alpha_{x2}D_2E_2 + \alpha_{x3}D_3E_3 + \\ &\quad \alpha_{x4}D_4E_4 + \alpha_{x5}D_5E_5 + \alpha_{x6} \\ p_y &= \alpha_{y1}D_1E_1 + \alpha_{y2}D_2E_2 + \alpha_{y3}D_3E_3 + \\ &\quad \alpha_{y4}D_4E_4 + \alpha_{y5}D_5E_5 + \alpha_{y6} \\ p_z &= \alpha_{z1}D_1E_1 + \alpha_{z2}D_2E_2 + \alpha_{z3}D_3E_3 + \\ &\quad \alpha_{z4}D_4E_4 + \alpha_{z5}D_5E_5 + \alpha_{z6} \end{aligned} \tag{2}$$

In a further reduced model, only three signals were used. (Equation 3) As can be seen in Figure 2, there were two sensors positioned to measure shear in the x-direction and two more for the y-direction. In the three sensor model, two of the redundant sensors were ignored.

$$\begin{aligned} p_x &= \alpha_{x1}D_2E_2 + \alpha_{x2}D_3E_3 + \alpha_{x3}D_5E_5 + \alpha_{x4} \\ p_x &= \alpha_{y1}D_2E_2 + \alpha_{y2}D_3E_3 + \alpha_{y3}D_5E_5 + \alpha_{y4} \\ p_x &= \alpha_{z1}D_2E_2 + \alpha_{z2}D_3E_3 + \alpha_{z3}D_5E_5 + \alpha_{z4} \end{aligned} \tag{3}$$

B. Results

1) Load Sensitivity: Figure 7 shows the response of the three sensors to loads in x (shear), y (shear), and z (normal). Sensor 3 had a sensitivity of approximately -15.7mV/kPa to shear loads in x while sensors 5 and 2 had sensitivities of approximately 0mV/kPa and 0.7mV/kPa, respectively. Sensor 2 had a sensitivity of approximately -19.4mV/kPa to shear loads in y while sensors 5 and 3 both had sensitivities of approximately 0mV/kPa. Sensor 5 had a sensitivity of approximately -0.58mV/kPa to normal loads in z while sensors 2 and 3 had sensitivities of approximately -0.44mV/kPa and -0.96mV/kPa, respectively, although both contained significant nonlinearities in their responses to moderate normal loads. The hysteresis of sensors 2, 3, and 5 was approximately 10%, 9%, and 7%, respectively.

2) Cyclic Drift: Figure 8a shows the response of sensor 5 to 10 loading and unloading cycles at the beginning of the cyclic drift test and 10 loading and unloading cycles at the end of the test. The sensor response drifted approximately 50mV over the 2 hour test. The sensitivity at the beginning was -0.28mV/kPa and the sensitivity at the end was -0.26mV/kPa. The taxel used for this test was of slightly different construction than that used for the sensitivity measurements, and had a lower sensitivity to normal loads.

3) Static Drift and Thermal Sensitivity: Figure 8b shows the response of sensor 5 to a static load over approximately 16 hours. The sensor response drifted approximately 32mV over the 16 hour test. Figure 8c shows the same data as a function of ambient temperature. The sensor had a thermal sensitivity of approximately 11mV/°C. This is consistent with the value found on the datasheet for the sensor. Figure 8b also shows the static drift when temperature effects were removed. In this case, the static drift was approximately 4mV.

4) Dynamic Response: Figure 8d shows the response of sensor 5 to a step-like load in time and the z axis load as measured by the ATI force sensor. The load reflects the contact pressure on the top surface of the silicone, while the sensor voltage reflects the translation of an internal, reflective boundary. Two notable features of data can be explained by viscoelastic effects: 1) sensor 5 lagged the ATI signal on the upward slope of the curve and 2) the ATI signal relaxed by approximately 10kPa on the plateau.

5) Modeling results: Figure 6 demonstrates the sensitivities of each of these terms to a varying x load at a fixed normal pressure. Plots in a row in this figure are from a common detector; and plots in a column are from a common emitter. Plots on the diagonal represent the self emitter/detector signal (those signals which were characterized in the previous section of this paper). Off-diagonal terms are detector responses to other emitters. The figure demonstrates that some of the non-self emitter/detector combinations provide information to shear forces, and, though less sensitive than the self-illuminated terms, may contribute to the more accurate measurement of force.

All 78 coefficients in the 25-signal model (Eq. 1) were calculated using data collected during one trial, and the model's accuracy was evaluated by applying the coefficients obtained to the data from a second trial. The optical sensor signals recorded during the validation trial were used as inputs to the model, and the pressure predicted by the model was compared against that measured with the load cell. A characteristic comparison is shown in figure 9, showing optical sensor results along with load cell results. Shear determination was accurate to an root-mean-square (rms) error of 2.4kPa in x and 3.2kPa in y for the representative trial displayed in figure 9. The rms error for the normal pressure was 11.4kPa.

The coefficients for the five signal (Eq. 2) and three signal models (Eq. 3) were calculated as well. The data collected for evaluating the reduced-order models was different than the data collected for evaluating the 25 signal model in several ways. For the reduced-order models, the forces were applied by hand, rather than by turning the knobs on a three-axis stage. This resulted in data that was more complex (it changed simultaneously in multiple axes) and

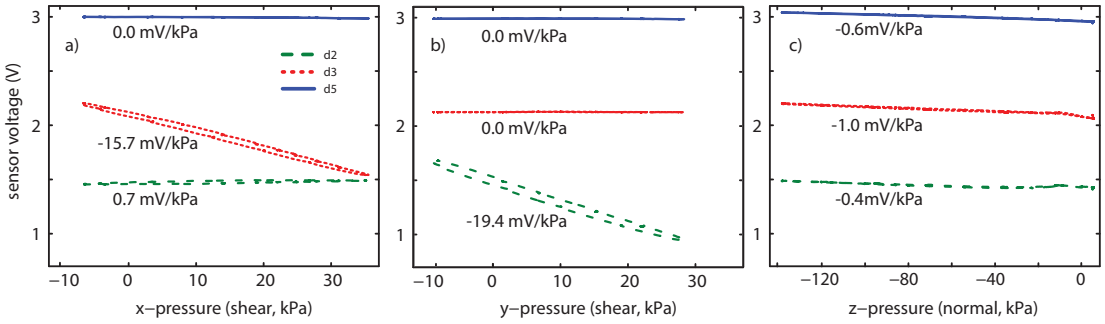

Fig. 7. Sensor responses to loading in the directions indicated, with approximate sensitivities.

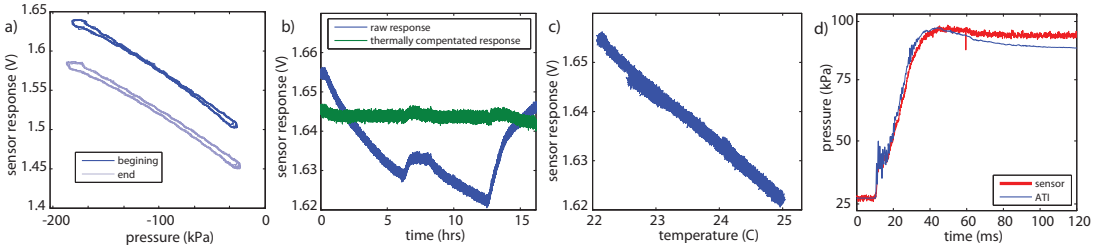

Fig. 8. a) Sensor 5 response to cycling in the z (normal) axis. 10 cycles at the beginning of the test (dark blue) differ from 10 cycles after approximately 2 hours (light blue). b) Sensor 5 response in time subject to a static load in the z-axis. c) Sensor 5 response to changes in ambient temperature. d) Sensor 5 response in time to a step-like load in the z-axis and the z-axis load as measured by the ATI force sensor.

model	25 signal	5 signal	3 signal
x (shear) error	2.4 kPa	4.0 kPa	4.4 kPa
y (shear) error	3.4 kPa	5.3 kPa	5.6 kPa
z (normal) error	11.4 kPa	12.6 kPa	12.6 kPa

TABLE I

MODELING ERRORS IN EACH OF THREE AXES.

of lower magnitude (the stages had greater force-production capabilities than the investigators' hands). While this made direct comparison between the data challenging, it did result in data with characteristics similar to those expected in robotics and prosthetics applications. Additional differences were introduced in the analysis of the data. For the reduced-order models, 10 data sets were collected, and the models were evaluated using leave-one-out-cross-validation. They were trained on 9 of the data sets, and tested on the tenth, and this process was repeated for each of the ten data sets. The results were then averaged together.

As a result of these differences, comparisons between the 25 signal model and the reduced-order models must be made with caution. However, comparison is still instructive. The error in all three models is summarized in Table I.

The reduced-order models showed a somewhat lower performance (higher rms error) than the full 25 signal model. This is not surprising, since the 25 signal model makes use of more information, although for reasons mentioned earlier care should be taken in interpreting this difference. Particularly interesting is the comparison between the five signal and three signal models. The performance difference is relatively small, even indistinguishable in the case of normal loads.

C. Discussion

The taxel's sensitivity in measuring shear suggests that it may be a viable sensor for use in robotic and prosthetic tactile sensing applications. Its normal sensitivity was more than an order of magnitude lower. Its potential usefulness as a sensor for normal loads has yet to be established, however our experience with the device gives encouragement that its normal sensitivity can be improved and its error in predicting normal forces decreased.

The taxel drifted about 35kPa over the course of 2 hours of cyclic loading. Though we did not record temperature during this experiment, the information we gathered from the static drift experiment leads us to believe that the cyclic drift observed was largely due to temperature. During the static drift experiment, we measured the ambient temperature and the data show that the drift observed can be attributed almost entirely to thermal fluctuation. We suspect that by incorporating the taxel's thermal sensor into the postprocessing of its sensor measurements, we can eliminate the cyclic and static drift. As shown in the characterization of the dynamic response, the sensor had a significant response lag. The lag had no significant pure delay component, but consisted of viscoelastic-like behavior, almost certainly due to the silicone

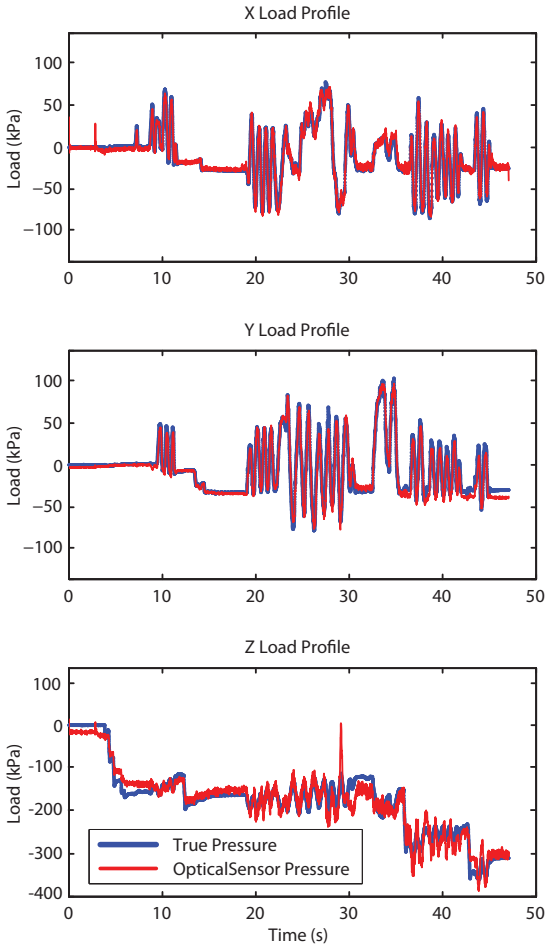

Fig. 9. Load profile showing truth and optical sensor load measurement in all three axis

in its structure.

All three linear models provided reasonable pressure measurement performance. Surprisingly, the reduced-order models performed on par with the full 25 signal model. This has implications for the design of future generations of the sensor. Using three sensors instead of five will make taxels cheaper, smaller, and easier to fabricate. Using three signals instead of 25 will decrease the taxel's information demands, increasing its sampling rate and the amount of data the can be transmitted, processed, and stored or any given system.

The greatest opportunity for improving the taxel is in its sensitivity to normal loads. We plan to address this in two ways: 1) by making the sensor more sensitive to compression and 2) by refining the model of its operation. Preliminary data suggests that the sensitivity of the taxel to normal loads is highly dependent on the thickness of the transparent silicone (the clear resilient layer in Fig. 3). Thinner silicone appears to yield more sensitive taxels. The taxels evaluated in this paper all had a clear silicone thickness of 1-1.5mm. An initial analysis suggests that a 0.5mm-thick layer may yield normal sensitivities that are higher by a factor of 2-5.

We also plan to refine the model of the sensor beyond the linear models discussed above. Temperature compensation was not applied to these validation studies, but we have shown that it is an important component of error in environments where temperature is not controlled. And we have not yet examined models in which the three axes are dependent on one another. But likely the most important improvement we can make to our models is to explicitly account for hysteresis. The failure of the taxel to behave linearly is evident in the single-axis characterizations (see Fig. 7) and even in that simple case was responsible for a significant amount of error. By explicitly accounting for hysteresis in a model that retains a small amount of sensor history, we plan to reduce the error in all three sensing axes.

IV. ACKNOWLEDGMENTS

The authors would like to thank Jeff Dabling for assistance with the drift tests and Larry Anderson for assistance with the PCD design and fabrication. This work was funded in part by DARPA and the Congressionally-Directed Medical Research Program.

REFERENCES

[1] J. Ulmen and M. Cutkosky, "A robust, low-cost and low-noise artificial skin for human-friendly robots," *IEEE/RSJ International Conference on Intelligent Robots and Systems*, pp. 4836-4841, 2010.

[2] Y. Ohmura, A. Nagakubo, and Y. Kuniyshi, "Conformable and scalable tactile sensor skin for curved surfaces," *Proc. of the 2006 IEEE Int. Conf. on Robotics & Automation*, pp. 1348-1353, 2006.

[3] A. Dollar, C. R. Wagner, and R. D. Howe, "Embedded sensors for biomimetic robotics via shape deposition manufacturing," *Proceedings of the first IEEE/RAS-EMBS International Conference on Biomedical Robotics and Biomechatronics*, 2006.

[4] G. I. Rowe and A. V. Mamishev, "Simulation of a sensor array for multi-parameter measurements at the prosthetic limb interface," *PIE 9th Annual International Symposium on NDE for Health Monitoring and Diagnostics*, vol. 5394, pp. 493-500, 2004.

[5] M. R. Cutkosky, R. D. Howe, and W. R. Provancher, *Springer Handbook of Robotics*, ch. Force and Tactile Sensors, pp. 455-476. Berling/Heidelberg, Germany: Springer-Verlag, 2008.

[6] J. Sanders and C. Daly, "Measurement of stresses in 3 orthogonal directions at the residual limbprosthetic socket interface," *IEEE Trans Rehabil Eng*, vol. 1, pp. 79-85, 1993.

[7] K. Noda, K. Hoshino, K. Matsumoto, and I. Shimoyama, "A shear stress sensor for tactile sensing with the piezoresistive cantilever standing elastic material," *Sensors and Actuators A*, vol. 127, pp. 295-301, 2006.

[8] P. Valdastri, S. Roccella, E. C. L. Beccai, A. Menciassi, M. C. Carrozza, and P. Dario, "Characterization of a novel hybrid silicon three-axial force sensor," *Sens. Actuators A*, vol. 123124, pp. 249-257, 2005.

[9] Y.-M. Huang, N.-C. Tsai, and J.-Y. Lai, "Development of tactile sensors for simultaneous, detection of normal and shear stresses," *Sensors and Actuators*, vol. 159, pp. 189-195, 2010.

[10] J. Missinne, E. Bosman, B. V. Hoe, G. V. Steenberge, P. V. Daele, and J. Vanfleteren, "Embedded flexible optical shear sensor," *Proc. IEEE Sensors*, pp. 987-990, 2010.

CHAPTER 4

AN ELASTOMERIC INSOLE FOR 3-AXIS GROUND REACTION FORCE MEASUREMENT

Lucas Samuel Lincoln[1], Stacy J. Morris Bamberg[1], Erin Parsons[1], Curt Salisbury[2], and Jason Wheeler[2]

1. Department of Mechanical Engineering, University of Utah
2. Intelligent Systems and Controls, Sandia National Laboratories

This paper is submitted to the 2012 IEEE EMBC/RAS International Conference on Biomedical Robotics and Biomechatronics.

An elastomeric insole for 3-axis ground reaction force measurement

Lucas Samuel Lincoln, Stacy J. Morris Bamberg, Erin Parsons, Curt Salisbury, and Jason Wheeler

Abstract— **Measurement of the ground reaction force vector is important in clinical gait analysis and biomechanics research, for example to enable inverse dynamic calculations. Instrumented insoles allow biomechanical data to be collected outside of the motion analysis laboratory in many environments. However, current insole-based approaches typically measure only the vertical component of the reaction force and the plantar center of pressure. This work describes the development and evaluation of a silicone insole capable of measuring the complete three dimensional reaction force vector. The insole is optically based and low-cost with no complex manufacturing requirements. Accuracy over five nominal gait trails is shown to be on the order of 10% of the force range, with mean errors of 10.7 N in the shear directions and 68.1 N in normal. The insole can provide a simple mobile platform that allows kinetic gait data to be collected in many environments while minimally affecting the wearer's gait.**

I. INTRODUCTION

Human motion analysis is an important tool for the identification and diagnoses of pathological gait disorders or abnormalities. Though there are a handful of motion analysis techniques of various technical sophistication, the modern motion analysis laboratory (MAL) typically shares a common set of equipment: a stereographic camera system for 3D linkage kinematics, with passive or active markers attached to the subject; one or more 3- or 6-axis force plates embedded in the floor for ground reaction force (GRF) and plantar center of pressure (CoP) measurement; a video camera for qualitative analysis; and an electromyography (EMG) recording system to estimate muscle activation.

This type of laboratory is valuable due to its ability to quantify joint kinematics, kinetics and muscle activity. The use of force plates and camera systems in a MAL has provided clinicians and researchers with a robust set of tools for analyzing human motion for nearly 30 years [1], [2]. Inverse dynamic analysis can be performed to calculate external joint forces and torques. Additionally, algorithms such as computed muscle control [3] can be used to estimate muscle forces. This approach has several advantages over competing methods for muscle force estimation, such as the use of embedded in-vivo transducer placement [4] which is prohibitively invasive and EMG measurement [5] which is most effective for large, superficial muscles. GRF measurement using force plates is the current state of the art for most kinetic motion analysis research.

Despite these advantages, there are some distinct disadvantages to the use of conventional MAL equipment. First, an external reference motion capture system, such as room-mounted force plates and cameras, limits motion capture to a laboratory setting. In these systems, the temporal amount of data which can be captured is limited by the subject's time in the laboratory and the spatial amount of data which can be captured is limited by the working volume of the laboratory. The range of gaits that can be captured is also limited by the environment; though stairs and ramps can be instrumented, common household and workplace obstacles must be brought in and adapted to function with a force plate to simulate daily tasks [6], [7], [8].

Additionally, the biomechanics of the foot are difficult to analyze in these systems because force plate data capture the GRF from the CoP of the shoe sole rather than the foot. Different types of shoes can affect the gait parameters and change the plantar pressure distribution on the foot [9]. Measuring the pressure distribution inside the shoe can allow a more direct, accurate, and detailed measurement of the foot plantar pressures and allow more accurate analysis of the biomechanics of the foot joints and muscles.

Finally, in order to evaluate the chronic effects of gait disorders or parameters, motion capture must take place often, or over long time scales. Ideally, data can be captured in the everyday environment of the subject to evaluate the effects of stairs, ramps, terrain and obstacles on gait characteristics. The authors assert that a low cost, external-reference free, and mobile motion analysis system holds immense value for motion analysis; as well as asserting that an insole-based solution is preferred. Mobile kinematic gait analysis systems have been developed but kinetic measurement systems are immature relative to MAL technology.

Several instrumented insoles and shoes are available for vertical GRF and CoP measurement. The GaitShoe (Massachusetts Institute of Technology, Boston, MA, USA) has been shown to estimate vertical GRF using force-sensitive-resistors (FSRs) [10]. CoP has also been estimated with the LEAFS (University of Utah, Utah, USA) insoles using FSRs and validated against force plate data [11]. The Parotec System (Paromed Medizintechnik, Neubeuern, Germany) insole uses 24 microsensors embedded within a hydrocell to obtain CoP data [12]. The BioFoot (Instituto de Biomecanica de Valencia, Valencia, Spain) contains 64 piezoelectric sensors to acquire detailed plantar pressure distributions [13]. The F-scan (Tekscan Inc., Boston, MA, USA) uses 960 pressure sensors for an insole measurement system, which has been

L.S. Lincoln and E. Parsons are students in the Bioinstrumentation Lab at the University of Utah, Salt Lake City, UT 84101 {lucas.lincoln, e.parsons}@utah.edu

Stacy Bamberg is an assistant professor at the University of Utah, Salt Lake City, UT 84101 sjm.bamberg@utah.edu

Jason Wheeler and Curt Salisbury are with the Intelligent Systems Controls Department, Sandia National Laboratories, Albuquerque, NM 87123 {jwwheel, cmsalis}@sandia.gov

used to detect GRF events such as initial contact and toe-off [14].

Insole technology for measuring shear forces began with magneto-resistive sensor technology in the fore-aft direction [15] and later adapted to measuring shear forces in two directions [16] in the 1980's. The magneto-resistive transducers can be coupled with load cells to obtain three-axis GRF with an insole [16]. The Kent Shear System (Kent University, Canterbury, UK) developed a bi-axial shear stress insole measurement system using piezoelectric resistors [17]. These shear insoles are constructed using cork and leather that are the same thickness as the transducer, so the subject's foot can come in direct contact with the shear transducer.

The XSens ForceShoe (XSens Technologies, Enschede, Netherlands) uses MEMS 3D inertial sensors in combination with load cells in an instrumented shoe to acquire three-axis GRF and CoP [18]. The ability of the ForceShoe to measure the GRF in three directions has significantly improved mobile motion analysis. However, the instrumented shoe design may alter the wearer's gait, must be fit carefully and is expensive. The insole Parotec System has the capability to measure three-axis GRF using the shear modulus of elasticity of the hydrocell [19] but, has not yet been successfully implemented in research due to the sensitivity of the sensor locations [12]. The M3D system (Doshisha University, Kyoto, Japan), uses small, mobile force plates and inertial measurement units (IMU) attached externally to various shoe types and sizes to measure three-axis GRF and CoP [20].

The insoles developed from previous research have been shown to accurately measure vertical GRF and plantar CoP. There is a need to measure three-axis GRF in order to accurately use inverse dynamics to resolve the joint kinetics and muscle forces. Although the instrumented ForceShoe can measure three-axis GRF, its applicability is limited by its high cost, limited range of shoe types/sizes and potential confounding effects on the wearer's gait. The work presented in this paper describes a novel, low-profile insole for measuring three-axis GRF and CoP with low cost tactile sensors, embedded in a silicone mold that can be adapted to various shoe types and sizes.

II. INSOLE DEVELOPMENT

The present work describes an elastomeric insole consisting of five 3-axis optical tactile sensor sites. The sensors are mounted on a flexible printed circuit board (PCB) and are embedded in silicone so as to not be felt by the wearer. The insole can be placed in most shoes within minimal effect on comfort or performance. The details of the sensors and insole are provided below.

A. Sensor Principal of Operation

The sensor uses reflected light intensity to detect the proximity of a reflective material. As a normal load is applied to the reflective material, the interstitial transparent material compresses and the reflective material moves closer to the light source (emitter) and light sensor (detector). This causes the detector to detect increased reflected light from the emitter. (See Fig. 1a and 1b) Shear loads are sensed by adding absorptive regions to the reflective layer. An applied shear load changes the ratio of absorptive to reflective material between the emitter and the detector. The changes the amount of light reflected back to the detector. (See Fig. 1c and 1d)

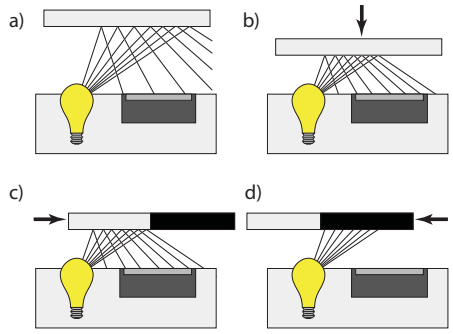

Fig. 1. The optical sensor's operating principle. a)-b) Normal loads move the reflective surface closer to the emitter, increasing the intensity of the light at the detector. c)-d) Shear loads move the absorptive portion of the polymer relative to the emitter, changing the intensity of the light at the detector.

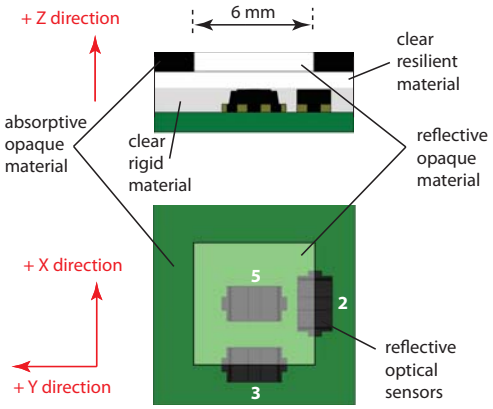

Fig. 2. Configuration of five photomicrosensors embedded in a silicone insole covered with a silicone mask.

B. Sensor Construction

The tactile sensor uses photomicrosensors (EE-SY199, Omron Corporation, Kyoto, Japan) containing a light emitter and detector. The emitter is potted in optically clear epoxy (ES1902 Hysol, Locktite, Henjel, Dusseldorf, Germany) and a clear layer of silicone rubber (Dragon Skin FAST, Smooth-On, Inc, Easton, Pennsylvania) is adhered atop the sensor. Attached to the top of the clear, resilient silicone layer is an opaque silicone layer with a pattern of absorptive (black) and reflective (white) areas. Utilizing 5 photomicrosensors, and designing the geometry of the microsensor layer and silicone mask, the sensor responds to strain in the elastomer in three

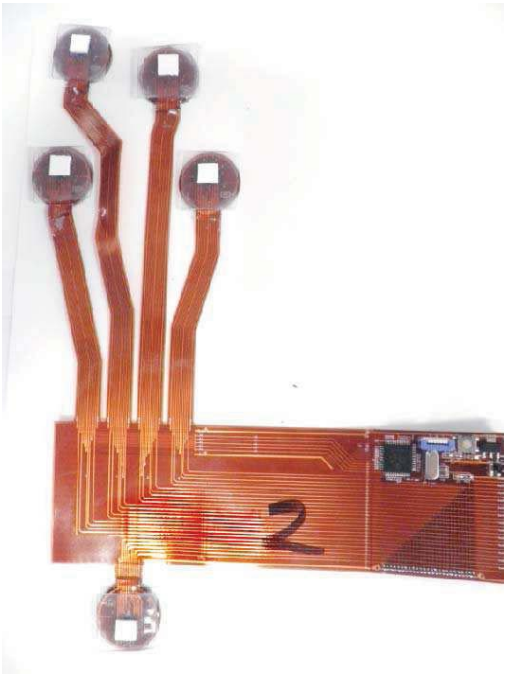

Fig. 3. Photo of the insole constructed, with silicone features above the sensor sites, not yet molded.

directions with limited coupling between axes (see figure 2).

If all the emitters are on simultaneously, some of the detectors saturate. Therefore, the emitters are pulsed such that one emitter is on for 1ms, followed in sequence by each other emitter. Each emitter illuminates all detectors to some degree. This provides 25 different signals over 5ms for a 5 sensor array (5 pulsed emitters illuminating 5 detectors.)

C. Insole Construction

The insole was designed to utilize multiple instances (taxels) of the sensor described in the previous section. Each taxel is a 5 photomicrosensor layout as described in the previous section. Taxel positions within the shoe are based on the work in [10] and [11], which enables accurate determination of CoP. The insole was designed on a flex circuit which is then molded into silicone to produce the insole. Each taxel is first covered in epoxy up to the top of the photomicrosensors. A thin (1-2 mm) layer of clear silicone is then molded and bonded to the top of the epoxy layer. Finally, the opaque silicone layer, with white squares directly over the microsensor array and black everywhere else, is molded directly to the top of the clear silicone. Because the silicone layers are identical (other than the color) the bond between these layers is excellent. The opaque layer can be very thin. In the insole used in the present work, the opaque layer was about 2mm, resulting in a total insole thickness of about 5.5mm.

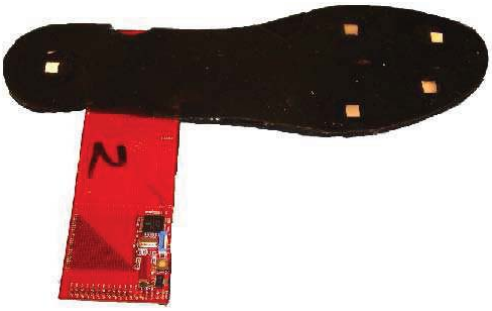

Fig. 4. Photo of the insole constructed and molded, ready for insertion into the shoe.

The insole with masks attached above the taxels is shown in figure 3. Note there is a header on the back of the insole on the lateral side of the shoe used to output the analog signals to the data acquisition system (DAQ). Fig. 4 displays the insole molded in silicone and ready for insertion into the shoe.

D. Training and Validation

As mentioned above, each taxel produces 25 unique signals related to the three-axis force measurement. With 5 taxels in this iteration of the insole, 125 total signals are produced. A linear least squares regression is used to train a model of the form:

$$\begin{aligned} Force \quad &= \alpha_1 D1E1 + \alpha_2 D1E2 + \alpha_3 D1E3 \\ &+ \alpha_4 D1E4 + ... + \alpha_{124} D125E4 \\ &+ \alpha_{125} D125E5 + \alpha_{126} \end{aligned} \tag{1}$$

where $D1E1$ is the response of detector 1 to emitter 5, and each α is a regression coefficient.

Coefficients are determined through a regression using at least 3 aggregate trials unique from the validation dataset.

III. EXPERIMENTAL PROCEDURE

A MAL was used for ground-truth measurement of the parameters of interest and was outfitted with a stereographic camera system (VICON, Oxford, UK) capable of sub-millimeter, 3D, passive, marker tracking, captured at 100Hz. In addition, the lab floor is outfitted with a ATMI OR6-7-2000-TT force plate with a resolution of 2.6lb over a range of 1000lb within a 18.25 x 20 x 3.25 in workspace. Force plate data werwe sampled at 1 kHz. The insole data were captured using a 16bit National Instruments (Austin, TX, USA) DAQ at 8kHz.

Tests on a single subject with the insole inside a common sneaker were performed. The shoe requires no alteration and, qualitatively, the insole imparts no unusual fit to the subject. A marker coordinate system was attached to the shoe to provide a transformation between shoe and MAL frames for sensor training purposes. The shoe, with the insole and marker system, is shown in Fig. 5. Note that the coordinate system markers are only required for the sensor training and

Fig. 5. Picture of insole in common shoe, with markers attached to examine angular deviations. Note the insole header passing out the lateral side of the ankle.

validation; and not for common data capture in the insole's end-use. The subject walked forward and backward across the force plate at a natural cadence. Each trial consisted of 6-8 steps (half forward, half reverse) and a total of 5 trails were analyzed. Manual synchronization of the MAL and insole data was performed in post-processing; a series of impulses were imparted by stomping quickly on the force plate at the start and end of the trial to provide temporal markers for alignment.

Though the insole develops 125 signals in time, a number of the traces on the flex circuit had intermittent connectivity issues as a result of poor layout and construction in this initial prototype. Unreliable signals are not included in the regression of validation, reducing the number of contributing signals (to a minimum of 97).

IV. RESULTS

Error was computed as the magnitude of the difference of the force measurements taken from the insole and the force plate.

The mean and standard deviation of error in each trial are displayed in Table I. Trials are listed in chronological order. Likewise, Table II displays the error as the percentage of the range of forces measured with the ground-truth force plate.

TABLE I
DIRECTIONAL ERRORS ON ALL 5 TRIALS, IN NEWTONS.

Trial	X (N)	Y (N)	Z (N)
1	25.85 ± 45.71	9.43 ± 12.53	72.31 ± 121.01
2	9.61 ± 16.52	6.54 ± 10.33	66.30 ± 119.75
3	11.40 ± 17.46	7.25 ± 11.42	72.47 ± 106.40
4	9.97 ± 16.77	7.41 ± 10.15	64.76 ± 94.44
5	11.90 ± 18.26	7.94 ± 10.53	64.64 ± 94.29

Fig. 6 presents the result of a particular trail, trained on the aggregate of all other trials. Time between approximately 8 seconds and 18 seconds are the alternating forward and reverse steps across the force plate. Times outside this range contain impulses used to synchronize data. The mean errors

TABLE II
DIRECTIONAL ERRORS ON ALL 5 TRIALS, IN PERCENT OF TRUE FORCE.

Trial	X	Y	Z
1	$11.07\% \pm 19.6\%$	$6.13\% \pm 8.14\%$	$12.02\% \pm 16.8\%$
2	$3.67\% \pm 6.31\%$	$4.29\% \pm 6.79\%$	$8.81\% \pm 15.92\%$
3	$3.34\% \pm 5.12\%$	$3.48\% \pm 5.48\%$	$7.65\% \pm 11.23\%$
4	$3.49\% \pm 5.87\%$	$3.14\% \pm 4.30\%$	$8.57\% \pm 12.49\%$
5	$2.94\% \pm 4.51\%$	$4.02\% \pm 5.33\%$	$6.21\% \pm 9.06\%$

in the trail presented in Fig. 6 were 3.5%, 3.1%, and 8.6% of the range in X, Y and Z, respectively.

Likewise, fig. 7 presents the result of another trial, again trained on the aggregate data of all other trails. In this plot, the synchronization pulses are not shown. The mean errors in Fig. 7 were 2.9%, 4.0%, and 6.2% in X, Y, and Z, respectively.

V. DISCUSSION AND CONCLUSIONS

The results demonstrate successful proof-of-concept measurement of three degree-of-freedom GRF in an insole-based system. Mean errors were within 10% of the range in these trials. This level of accuracy is somewhat lower than load-cell based systems. However, the insole system is less expensive, easier to manufacture, and should have a very small effect on the user's gait. Chronic gait GRF monitoring is possible with the system described, and it may be particularly useful for gait characterization outside of the laboratory environments.

It is interesting to note that the relative errors in all three directions are similar. The tactile sensors used in the present work are known to be much more sensitive to shear loads than normal loads (approximately one order of magnitude). The magnitude of the GRF in the vertical direction is much larger than the anterior/posterior and medial/lateral directions. These two factors result in the sensor error being somewhat uniform (as a percent of the true force).

Several known issues with the current system contribute to the error. The most evident is the analog continuity in the current layout of the flex-circuit. As mentioned previously, a number of sensors are shorted intermittently in-shoe, reducing the number of signals with which to determine force. This will be solved in future iterations with on-board digitization. Synchronizing the force plate and insole data for training and validation is currently performed by hand and, as such, has inherent repeatability and precision problems. Future work will incorporate simultaneous data capture on one machine to reduce this variability. In the tactile sensor design and characterization, the sensor is shown to have temperature dependence, however the insole as constructed does not contain temperature monitoring or compensation. This is a possible avenue of improvement. Other possible improvements which we are exploring include more sensor sites, repositioning of sensors, alternative insole thickness, silicones of different durometer and more advanced training models that incorporate nonlinearity and hysteresis.

VI. ACKNOWLEDGEMENTS

The authors would like to acknowledge Larry Anderson and Jeff Dabling at Sandia National Laboratories for their

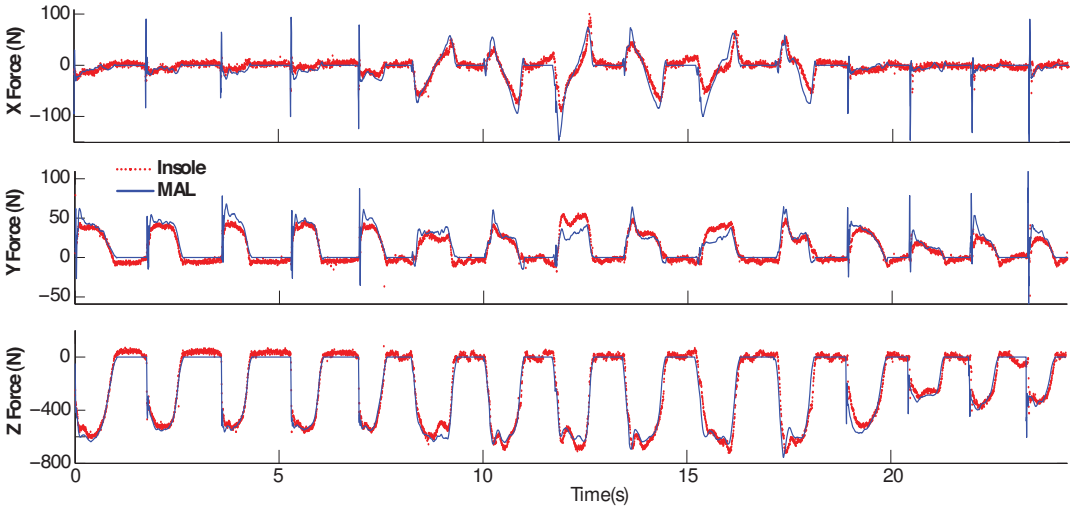

Fig. 6. Results from an in-shoe trial

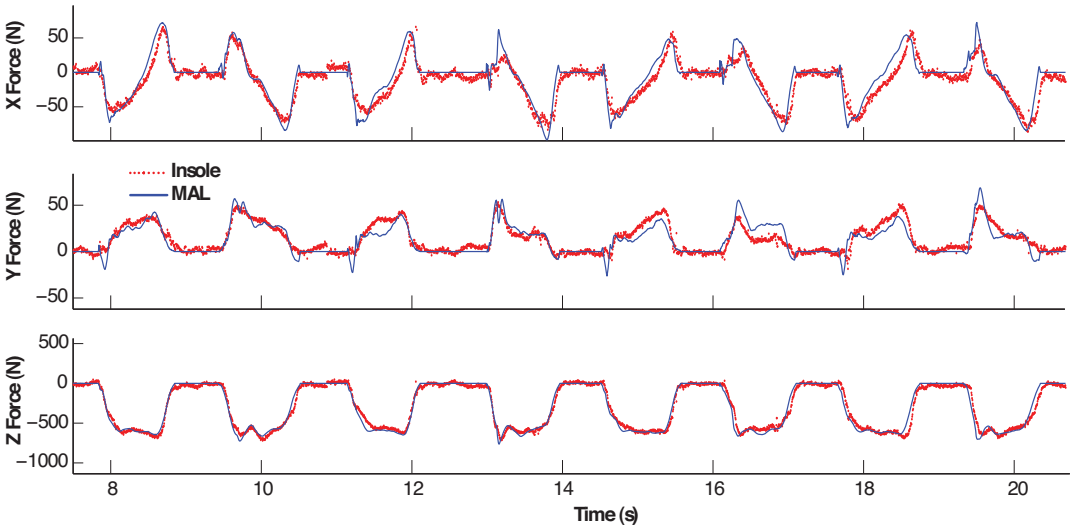

Fig. 7. Results from an in-shoe trial, only forward and reverse steps across plate.

support in sensor design and manufacture; as well as Bo Foremen of the University of Utah College of Health for his continued support in motion capture. Brandon Rohrer at Sandia National Laboratories assisted with editing the mansucript and figures.

Erin Parsons is supported in part by the National Science Foundation under Grant No. DGE-0654414(IGERT: Interdisciplinary Research Training in Biocentric Robotics).

REFERENCES

[1] G. W. Pratt Jr and J. T. O'Connor Jr, "Force plate studies of equine biomechanics," *Am J Vet Res*, vol. 37, no. 11, pp. 1251-1255, Nov. 1976.

[2] N. C. Heglund, "A Simple Design for a Force-plate to Measure Ground Reaction Forces," *J Exp Biol*, vol. 93, pp. 333-338, Mar 1981.

[3] D. G. Thelen, F. C. Anderson, and S. L. Delp, "Generating dynamic simulations of movement using computed muscle control," *J of Biomech*, vol. 36, pp. 321-328, 2003.

[4] P. V. Komi, "Relevance of in vivo force measurements to human biomechanics," *J of Biomechanics*, vol. 23, supp. 1, pp. 23-34, 1990.

[5] Y. Koike and M. Kawato, "Estimation of dynamic joint torques and trajectory formation from surface electromyography signals using a neural network model." *Biol Cybern*, vol. 73, no. 4, pp. 291-300, Sep. 1995.

[6] S. J. Dixon, A. C. Collop, and M. E. Batt, "Surface effects on ground reaction forces and lower extremity kinematics in running," *Med Sci Sports Exerc*, vol. 32, no. 11, pp. 1919-1926, 2000.

[7] P. A. Costigan, K. J. Deluzio, and U. P. Wyss, "Knee and hip kinetics during normal stair climbing," *Gait and Posture*, vol. 16, pp. 31-37,

2002.

[8] B. Yu, E. S. Growney, F. M. Schultz, and K. An, "Calibration of measured center of pressure of a new stairway design for kinetic analysis of stair climbing," *J of Biomechanics*, vol. 29, no. 12, pp. 1625-1628, 1996.

[9] T. G. McPoil Jr, "Footwear," *J of Phys Therap*, vol. 68, no. 12, pp. 1857-1865, Dec. 1988.

[10] S. J. M. Bamberg, A. Y. Benbasat, D. M. Scarborough, D. E. Krebs, and J. A. Paradiso, "Gait Analysis Using a Shoe-Integrated Wireless Sensor System," *IEEE Trans on Info Tech in Biomedicine*, vol. 12, no. 4, pp. 413-423, Jul 2008.

[11] P. S. Dyer and S. J. M. Bamberg, "Instrumented Insole vs. Force Plate: A Comparison of Center of Plantar Pressure," presented at the *IEEE Eng in Med and Bio Conf*, Boston, MA, USA, Sept 2011.

[12] K. J. Chesnin, L. Selby-Silverstein, and M. P. Besser, "Comparison of an in-shoe pressure measurement device to a force plate: concurrent validity of center of pressure measurements," *Gait and Posture*, vol. 12, pp. 128-133, 2000.

[13] A. Martínez-Nova, J. C. Cuevas-García, J. Pascual-Huerta, and R. Sánchez-Rodríguez, "BioFoot in-shoe system: Normal values and assessment of the reliability and repeatability," *The Foot*, vol. 17, pp. 190-196, Apr 2007.

[14] P. Catalfamo, D. Moser, S. Ghoussayni, and D. Ewins, "Detection of gait events using an F-Scan in-shoe pressure measurement system," *Gait & Posture*, vol. 28, pp. 420-426, Jan 2008.

[15] J. P. Pollard, L. P. Le Quesne, and J. W. Tappin, "Forces under the foot," *J of Biomed Eng*, vol. 5, no. 1, pp. 37-40, Jan 1983.

[16] M. Lord, R. Hosein, and R. B. Williams, "Method for in-shoe shear stress measurement," *J of Biomed Eng*, vol. 14, no. 3, pp. 181-186, May 1992.

[17] F. Akhlaghi and M. G. Pepper, "In-shoe biaxial shear force measurement: the Kent shear system," *Med Biol Eng Comput*, vol. 34, no. 4, pp. 315-317, Jul 1996.

[18] XSens Technologies, "The ForceShoe." [Online]. Available: http://www.xsens.com/en/general/forceshoe

[19] Parotec System instruction manual, Paromed Medizintechnik GmbH. 1997: Neubeuern, Germany.

[20] W. Adachi et al., "Development of Walking Analysis System Consisting of Mobile Force Plate and Motion Sensor," *33rd Annual Int Conf of the IEEE EMBS* , Boston, MA, USA, Aug 2011.

CHAPTER 5

CONCLUSIONS AND FUTURE WORK

5.1 Conclusions

This thesis describes the development and application of enabling improvements for an insole-base motion analysis laboratory.

Algorithmic improvements were applied to MEMS IMU motion tracking and reduced errors by an average of 99.55% over the same trails without the improvements. The low-cost calibration system was demonstrated to be relatively static, supporting its use in a clinical setting. The state estimation routine was tuned for gait analysis tested on normal walking and stair-climb trials. The 3-dimensional position of the foot in a typical walking gait and over stairs was tracked accurately with errors of approximately 10%.

A novel sensor was developed, constructed, and evaluated for measuring both shear and normal force in a low-profile package. It utilizes available components to remain low-cost and require no complex manufacturing. A regression technique and signal processing approach was developed for the sensor and validated over a series of tests – a single taxel of the design working as a tactile sensor provides pressure estimation accuracy greater than 1psi for both shear and normal.

With a novel 3 axis sensor developed, an insole was designed and constructed. The sensor fits comfortably within a common sneaker and requires no alteration. It is able to measure the 3-dimensional ground reaction force with an accuracy on the order of 10%, and is the only low-cost, insole-based system able to measure 3D GRF at this level.

5.2 Future Work

This document described work which serves as a proof-of-concept of new technologies required for an insole-based mobile motion analysis lab. There are vast improvements to be made in future iterations based on the principles described herein.

The IMU calibration routine and subsequent model could be improved by the inclusion of temperature compensation. MEMS IMU outputs are sensitive to temperature and compensating for these would continue to reduce errors. Additionally, the calibration hardware could increase in complexity somewhat (to include simple linear and angular measurement) to improve the accuracy of the model developed.

The zero-velocity-update algorithm could be vastly improved if made application-specific and incorporated into a GRF sensing insole. Using the shear and normal force measurement of the insole would enable a reliable identification of step, and likely even slip using shear force profiles, and one would not risk bias-updating during motion.

The tactile sensor developed could be optimized for the expected range of forces seen in normal gait by altering the dimensions of the sensor placement, mask geometry, and thickness and hardness of silicone.

Perhaps most importantly, the insole developed requires redesign to insure signal fidelity across all photomicrosensors. A system with digitization at each sensor site

would overall reduce board complexity and improve robustness. The insole should be redesigned to include digitization, and to incorporate IMU hardware for further studies of the proposed mobile motion analysis system as a whole.